Acta Crystallographica Section F
Structural Biology and Crystallization Communications
ISSN 1744-3091

Structure of a CRISPR-associated protein Cas2 from *Desulfovibrio vulgaris*

Poulami Samai, Paul Smith and Stewart Shuman*

Molecular Biology Program, Sloan–Kettering Institute for Cancer Research, USA

Correspondence e-mail: s-shuman@ski.mskcc.org

Received 8 September 2010
Accepted 5 October 2010

PDB Reference: Cas2, 3oq2.

CRISPRs (clustered regularly interspaced short palindromic repeats) provide bacteria and archaea with RNA-guided acquired immunity to invasive DNAs. CRISPR-associated (Cas) proteins carry out the immune effector functions. Cas2 is a universal component of the CRISPR system. Here, a 1.35 Å resolution crystal structure of Cas2 from the bacterium *Desulfovibrio vulgaris* (*Dvu*Cas2) is reported. *Dvu*Cas2 is a homodimer, with each protomer consisting of an N-terminal $\beta\alpha\beta\beta\alpha\beta$ ferredoxin fold (amino acids 1–78) to which is appended a C-terminal segment (amino acids 79–102) that includes a short 3_{10}-helix and a fifth β-strand. The $\beta5$ strands align with the $\beta4$ strands of the opposite protomers, resulting in two five-stranded antiparallel β-sheets that form a sandwich at the dimer interface. The *Dvu*Cas2 dimer is stabilized by a distinctive network of hydrophilic cross-protomer side-chain interactions.

1. Introduction

The prokaryal immune system known as CRISPR (clustered regularly interspaced short palindromic repeats) provides adaptive protection against foreign DNA elements (viruses and plasmids) as well as a heritable record of 'past genetic aggressions' (Barrangou *et al.*, 2007; Mojica *et al.*, 2005; Pourcel *et al.*, 2005). CRISPRs are present in nearly all archaea and about 40% of bacteria for which genome sequences are available (Karginov & Hannon, 2010; Sorek *et al.*, 2008; van der Oost *et al.*, 2009). CRISPRs consist of an array of short direct repeat sequences (25–50 bp) separated by hypervariable spacer sequences (20–70 bp). The repeat array is flanked on one side by an AT-rich region called the leader. CRISPR loci are surrounded by a set of conserved protein-coding *cas* (CRISPR-associated) genes that vary in their orientation and order (Haft *et al.*, 2005; Makarova *et al.*, 2006). Cas proteins carry out the immune effector functions, entailing the incorporation of new spacer sequences into the CRISPR locus, the processing of CRISPR RNAs and interference with the nucleic acid targets. The CRISPR locus is transcribed into a single RNA transcript with the leader at the 5′ end followed by the tandem repeats. The primary transcript is processed by a subset of the Cas proteins to generate unit-sized CRISPR RNAs (crRNAs; Brouns *et al.*, 2008), each consisting of one spacer flanked by 5′ and 3′ sequences derived from the direct repeats. The processed crRNAs can interfere with foreign genetic elements to which they display base complementarity (Horvath & Barrangou, 2010; Karginov & Hannon, 2010; Marraffini & Sontheimer, 2010; Sorek *et al.*, 2008; van der Oost *et al.*, 2009). The crRNA target can be either DNA or RNA, depending on the organism and the ensemble of Cas proteins (Brouns *et al.*, 2008; Hale *et al.*, 2009; Marraffini & Sontheimer, 2008).

The *cas2* gene is always located near a CRISPR locus. Although the role of *cas2* in CRISPR biology is not well defined, the available genetic studies indicate that *cas2* is not required for the synthesis of the pre-CRISPR transcript or its processing to crRNAs (Brouns *et al.*, 2008). Cas2 proteins are small (80–120 amino acids) and are conserved among CRISPR-bearing taxa. Crystal structures have been solved for four Cas2 proteins: the paralogs *Sso*1404 and *Sso*8090 from the crenarchaeon *Sulfolobus solfataricus* (PDB codes 2ivy, 2i8e and 3exc; Beloglazova *et al.*, 2008), *Pfu*1117 from the euryarchaeon *Pyrococcus furiosus* (PDB code 2iox) and *Tth*1823 from the

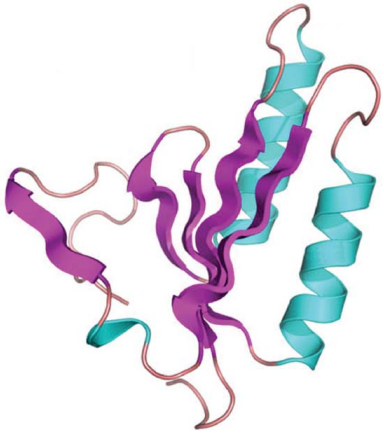

bacterium *Thermus thermophilus* (PDB code 1zpw). These Cas2s adopt a ferredoxin fold composed of a four-stranded antiparallel β-sheet plus two α-helices packed against one face of the sheet. Beloglazova *et al.* (2008) demonstrated metal-dependent endoribonuclease activity for the *Sso*1404 Cas2 protein. The *Sso*8090 paralog and the Cas2 homologs from *Thermotoga maritima*, *Methanobacterium thermoautotrophicum*, *Archaeoglobus fulgidus* and *Nitrosomonas europea* also had RNase activity. Mutational analysis identified six residues in *Sso*1404 as important for RNase activity; these were suggested to comprise the RNase active site. The potential roles of a Cas2 RNase in the CRISPR pathway might be to selectively degrade phage transcripts or to globally inhibit translation by mRNA cleavage (Beloglazova *et al.*, 2008).

Here, we report the 1.35 Å resolution crystal structure of *Dvu*Cas2 from the sulfate-reducing bacterium *Desulfovibrio vulgaris* Hildenborough. The sequenced *D. vulgaris* genome consists of a 3.57 Mb chromosome and a 202 kb megaplasmid (Heidelberg *et al.*, 2004). The *D. vulgaris* CRISPR and flanking *cas2* gene are located on the megaplasmid. To our knowledge, there have been no reports to date concerning the structure or function of CRISPR-system components from this organism.

2. Materials and methods

2.1. Purification of *Dvu*Cas2

The *D. vulgaris* Hildenborough *cas2* gene (DVUA0135; accession code YP_009175) was amplified by PCR from genomic DNA with sense and antisense primers that introduced a *Bam*HI site over the start codon and a *Not*I site 3′ to the stop codon. The PCR product was digested with *Bam*HI and *Not*I and inserted into pET-His$_{10}$Smt3. The resulting pET-DvuCas2 plasmid encodes the 102-amino-acid *Dvu*Cas2 protein fused to an N-terminal His$_{10}$Smt3 tag. Cultures (8 l) of *Escherichia coli* BL21 (DE3) pET-Cas2 were grown at 310 K in Terrific Broth containing 0.1 mg ml^{-1} kanamycin until A_{600} reached ∼0.8. The cultures were adjusted to 0.5 m*M* isopropyl β-D-1-thiogalactopyranoside and incubation was continued for 18 h at 290 K with continuous shaking. Cells were harvested by centrifugation and stored at 193 K. All subsequent procedures were performed at 277 K. Thawed cells were resuspended in 100 ml buffer *A* (50 m*M* Tris–HCl pH 7.5, 1.2 *M* NaCl, 200 m*M* $LiSO_4$, 15 m*M* imidazole, 10% glycerol) supplemented with 1% Triton X-100 and 1 mg ml^{-1} lysozyme to achieve cell lysis. The lysate was sonicated to reduce its viscosity and insoluble material was removed by centrifugation. His$_{10}$Smt3-Cas2 was isolated from the soluble extract by adsorption to 15 ml Ni–NTA agarose (Qiagen) that had been equilibrated in buffer *A*. The bound protein was eluted stepwise with 50, 100, 200, 350 and 500 m*M* imidazole in buffer *B* (50 m*M* Tris–HCl pH 8.0, 50 m*M* NaCl, 10% glycerol). The elution profile was monitored by SDS–PAGE of the column fractions. The 200 and 350 m*M* imidazole eluate fractions containing His$_{10}$Smt3-Cas2 were pooled (200 mg protein), supplemented with 300 µg Ulp1 (a Smt3-specific protease) and dialyzed overnight against buffer *C* (50 m*M* Tris pH 8.0, 250 m*M* NaCl, 5 m*M* DTT, 10% glycerol). The resulting mixture of cleaved His$_{10}$Smt3 and tag-less Cas2 was applied onto a 10 ml Ni–NTA agarose column that had been equilibrated with buffer *C*. Cas2 was recovered in the flowthrough fractions, devoid of His$_{10}$Smt3, which bound to the column. The Ni–agarose flowthrough material was applied onto a 10 ml column of DEAE-Sephacel that had been equilibrated with buffer *C*. Cas2 was recovered in the DEAE flowthrough fraction and was concentrated to a volume of 5 ml by centrifugal ultrafiltration. This material was applied onto a 120 ml HiPrep 16/60 Superdex-200 gel-filtration column equilibrated in 10 m*M* Tris–HCl pH 8.0, 100 m*M* NaCl, 1 m*M* DTT. The peak Cas2-containing fractions were concentrated by centrifugal ultrafiltration to 20 mg ml^{-1} in a 2 ml volume and the preparation was stored at 193 K.

Table 1
*Dvu*Cas2 crystallographic data and refinement statistics.

Standard definitions are used for all of the parameters. Values in parentheses are for the highest resolution bin. The data-collection statistics are from *SCALEPACK*. The refinement and geometric statistics are from *PHENIX*.

	Thimerosal-soaked crystal	Native crystal
Space group	*C*2	*C*2
Unit-cell parameters at 130 K (Å, °)	a = 107.30, b = 48.92, c = 41.61, β = 98.68	a = 107.88, b = 48.81, c = 41.32, β = 99.20
Radiation source	Cu $K\alpha$	APS 24-ID-E
Wavelength (Å)	1.5418	0.9795
Crystallographic data quality		
Resolution (Å)	25.0–2.30 (2.34–2.30)	50.0–1.35 (1.37–1.35)
R_{merge} [for $I > -3\sigma(I)$] (%)	9.3 (29.8)	4.9 (43.0)
Unique reflections†	18368 (909)	45550 (2001)
Mean multiplicity	3.35 (3.3)	3.50 (2.7)
Completeness (%)	99.2 (98.7)	97.0 (85.7)
Mean $I/\sigma(I)$	14.0 (3.8)	29.1 (2.0)
Phasing statistics		
Phasing method	Hg-SAD	—
Resolution (Å)	25.0–3.0	—
Anomalous signal‡	0.08	—
Figure of merit§	0.539/0.78	—
Refinement statistics		
Resolution (Å)	—	29.0–1.35 (1.40–1.35)
R_{work}/R_{free}¶ for $F > 0$	—	0.128/0.177 (0.174/0.249)
Estimated coordinate error (Å)	—	0.13
Model statistics		
R.m.s.d. bond lengths (Å)	—	0.006
R.m.s.d. bond angles (°)	—	1.12
NCS deviations†† [C^α residues] (Å)	—	0.316 [96]
Ramachandran outliers	—	0
B factors (Å^2)		
Wilson	—	12.1
Overall	—	24.3
Protein	—	22.1
Heteroatoms	—	35.9
Model contents		
Residues (chain *A*/chain *B*)	—	99/102
Alternate conformations	—	36
Heteroatoms	—	5 sulfate, 3 citrate‡‡, 1 Tris, 1 sodium, 1 chloride
Waters	—	299
PDB code	—	3oq2

† F^+ and F^- were treated as equivalent observations for native data sets, but as distinct in the data for the thimerosal-soaked crystal. ‡ Anomalous signal as output by *Phaser* using the formula $([\langle\|F(+)\| - \|F(-)\|^2\rangle]/\{1/2[\langle|F(+)|\rangle^2 + \langle|F(-)|\rangle^2]\})^{1/2}$. § Hg-SAD figures of merit are from *Phaser*/*RESOLVE*. ¶ The R_{free} sets for cross-validation consisted of 5% of data selected at random. †† No NCS restraints were used during refinement. ‡‡ Two sulfate positions are co-occupied by citrate.

2.2. Crystallization, diffraction data collection and structure determination

Crystallization was performed at room temperature by the hanging-drop vapor-diffusion method. Cas2 (1 µl) was mixed with an equal volume of reservoir solution consisting of 0.1 *M* trisodium citrate, 1 *M* lithium sulfate and 0.5 *M* ammonium sulfate. Plate-shaped crystals were harvested after 2–3 d and were transferred to a solution consting of 0.1 *M* trisodium citrate, 1 *M* lithium sulfate and 2 *M* ammonium sulfate prior to flash-freezing in liquid nitrogen. Alternatively, a Hg derivative was prepared by transferring crystals to the same solution containing 2 m*M* thimerosal for 30 min prior to flash-freezing in liquid nitrogen. Diffraction data for native crystals were collected to 1.35 Å resolution on APS beamline 24-ID-E at a wavelength of 0.9795 Å (200 consecutive 1° frames). Diffraction data

for the thimerosal-soaked crystal were collected to 2.3 Å resolution using a Rigaku R-AXIS IV detector and a rotating-anode Cu $K\alpha$ X-ray source at 1.5418 Å (208° of combined oscillation data). The data were processed using *HKL*-2000 and *SCALEPACK* (Otwinowski & Minor, 1997). The native and thimerosal-soaked crystals both belonged to space group *C*2 and had similar unit-cell parameters, but were nonisomorphous.

Single-wavelength anomalous diffraction (SAD) phasing calculations for the thimerosal-soaked crystal were implemented in *PHENIX*/*Phaser* (Adams *et al.*, 2002). Anomalous difference Fourier maps revealed four peaks above 10σ. The initial phases were improved in *RESOLVE* with the aid of noncrystallographic symmetry determined from the heavy-atom sites (Terwilliger, 2000, 2003). The *RESOLVE* map revealed two Cas2 molecules in the asymmetric unit and allowed the automatic building of ∼75% of the amino acids in the Cas2 protomers. The two mercury sites per Cas2 protomer were located adjacent to cysteine side chains, as expected.

This initial model was used to derive phases for the native Cas2 crystal, which were improved in *RESOLVE*. The structural model was extended with the autobuild feature of *PHENIX* and was then edited manually in *Coot* (Emsley & Cowtan, 2004) and refined iteratively against experimental data in *PHENIX* using refinement of individual sites, occupancy refinement for alternate conformations and anisotropic atomic displacement parameters. The final refined model at 1.35 Å resolution (R and $R_{\rm free}$ values of 0.128 and 0.177, respectively) included 99 and 102 amino acids from Cas2 protomers *A* and *B* with excellent geometry (Table 1).

3. Results and discussion

3.1. *Dvu*Cas2 structure and comparison with other Cas2 proteins

The *A* and *B* protomers of the *Dvu*Cas2 homodimer each consist of an N-terminal $\beta\alpha\beta\beta\alpha\beta$ ferredoxin fold (amino acids 1–78) to which is appended a C-terminal segment (amino acids 79–102) that includes a short 3_{10}-helix and a fifth β-strand (Figs. 1*a* and 1*f*). The tertiary structures of the *A* and *B* protomers were similar overall (r.m.s.d. of 0.32 Å at 96 C^{α} positions), though punctuated by many local variations, *e.g.* in the main-chain conformation of the $\beta1$–$\alpha1$ loop, in numerous side-chain orientations and the asymmetric association of sulfate ligands with one or the other subunit.

A *DALI* search with *Dvu*Cas2 identified the four known Cas2 structures as the highest scoring hits, as follows: *Tth*1823 (*Z* score 11.6; r.m.s.d. of 1.9 Å at 82 C^{α} positions), *Pfu*1117 (*Z* score 10.4), *Sso*8090 (*Z* score 10.2) and *Sso*1404 (*Z* score 9.3). These four Cas2 structures are superimposed on *Dvu*Cas2 and offset laterally in Figs. 1(*b*)–1(*e*). A structure-based alignment of the amino-acid sequences of *Dvu*Cas2, *Pfu*1117, *Tth*1823, *Sso*8090 and *Sso*1404 is shown in Fig. 1(*f*). These comparisons reveal several distinctive features of *Dvu*Cas2. For example, *Dvu*Cas2 is unique in having a 3_{10}-helix as the connecting secondary-structure element to the C-terminal segment (Fig. 1*a*); this contrasts with the α-helices found in the equivalent positions of *Sso*1404 (Fig. 1*b*) and *Sso*8090 (Fig. 1*e*) and the lack of any defined secondary structure at the corresponding sites in *Tth*1823 (Fig. 1*c*) and *Pfu*1117 (Fig. 1*d*). The $\beta1$–$\alpha1$ loop is longer in *Dvu*Cas2 than in any of its homologs (Figs. 1*a* and 1*f*). [Note that *Sso*1404 is distinguished by its longer $\alpha2$–$\beta4$ loop (Figs. 1*b* and 1*f*).] Finally, the paths of the C-termini distal to the equivalent of the *Dvu*Cas2 $\beta5$ strand vary among the Cas2 proteins. The C-terminus projects downwards in *Dvu*Cas2, *Tth*1823 and *Pfu*1117, but upwards in *Sso*1401 and *Sso*8090 (Figs. 1*a*–1*e*).

3.2. The *Dvu*Cas2 dimer interface

The $\beta5$ strands of the *Dvu*Cas2 *A* and *B* protomers project across a pseudo-twofold axis to align with the $\beta4$ strands of the opposite protomers, resulting in two five-stranded antiparallel β-sheets of topology $\beta5^{*}\beta4132$ that form a β-sandwich at the dimer interface (Fig. 2*a*). The dimer is stabilized by many hydrophilic cross-protomer side-chain interactions (Fig. 2*b*). Glu86 tethers $\beta5$ to the *trans* protomer *via* a salt bridge to Lys58 (in $\alpha2$) and a hydrogen bond to Tyr76 ($\beta4$). Arg73 and Tyr75 link $\beta4$ to the $\beta3$ and $\beta5$ strands and the

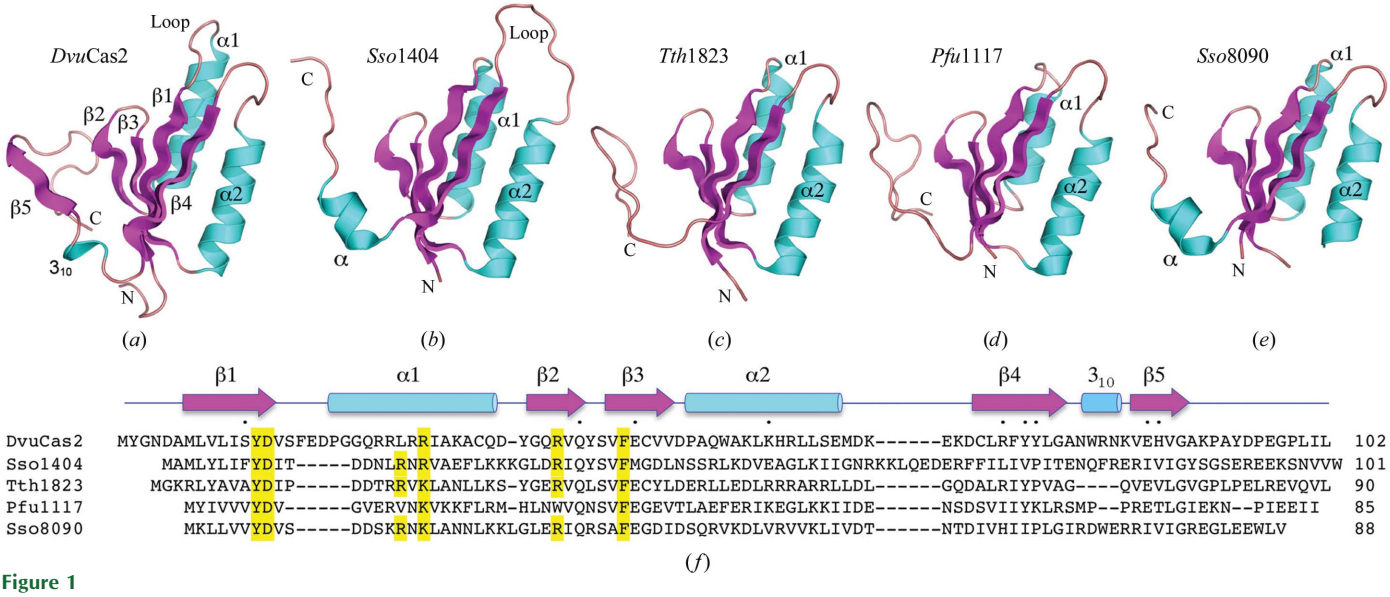

Figure 1
Structure of *Dvu*Cas2 and comparison to other Cas2 homologs. The fold of the *Dvu*Cas2 protomer (PDB code 3oq2) is shown in (*a*) with cyan helices and magenta β-strands. (*b*)–(*e*) show the tertiary structures of the Cas2 homologs *Sso*1404 (PDB code 2i8e), *Tth*1823 (PDB code 1zpw), *Pfu*1117 (PDB code 2i0x) and *Sso*8090 (PDB code 3exc) superimposed on *Dvu*Cas2 and then offset horizontally. The N- and C-termini are labeled. (*f*) shows a structure-based alignment of the amino-acid sequences of the five Cas2 proteins. The secondary-structure elements of *Dvu*Cas2 are shown above the sequence, with β-strands depicted as arrows and helices as cylinders. Gaps in the alignment are indicated by dashes. The amino-acid side chains that comprise the *Dvu*Cas2 homodimer interface (Fig. 2) are denoted by dots above the sequence. Residues that are essential for the endoribonuclease activity of *Sso*1404 are highlighted in yellow.

C-terminal peptide of the *trans* protomer *via* multiple hydrogen bonds to the Glu46 carboxylate, His87 N^{δ} and the Leu100 main-chain carbonyl (Fig. 2*b*). Gln41 tethers β2 to β1 and the β2–β3 loop of the *trans* protomer by hydrogen bonds to Ser12 O^{γ} and Ser43 O^{γ}, respectively (Fig. 2*b*). The side-chain atomic contacts at the *Dvu*Cas2 dimer interface are substantially different from those seen in the *Sso*1404 and *Sso*8090 structures, which is consistent with the lack of side-chain conservation at most of the residues that comprise the interface in *Dvu*Cas2. Many (though not all) of the cross-protomer contacts seen in *Dvu*Cas2 are conserved in *Tth*1183.

3.3. Does *Dvu*Cas2 have a phosphodiesterase active site?

*Sso*1404 was characterized as a metal-dependent endoribonuclease that incises single-stranded RNAs to yield 5′-phosphate and 3′-OH ends at the break site (Beloglazova *et al.*, 2008). Alanine scanning identified six *Sso*1404 residues that are essential for RNase activity (Tyr9, Asp10, Arg17, Arg19, Arg31 and Phe37); these are highlighted in yellow in Fig. 1(*f*). Five of the six essential *Sso*1404 residues are conserved in *Dvu*Cas2; they correspond to *Dvu*Cas2 Tyr13, Asp14, Arg28, Arg39 and Phe45 (Fig. 3). Beloglazova *et al.* (2008) speculated that five of the essential side chains (Tyr9, Asp10, Arg17, Arg31 and Phe37) could form a phosphodiesterase active site. They specifically proposed that (i) Asp10 is critical for catalysis because it coordinates the divalent-cation cofactor and (ii) the two Asp10 carboxylates, which are located 6.5 Å from each other at the *Sso*1404 homodimer interface, cooperate to bind a single divalent cation. This detailed mechanistic hypothesis is most unlikely to apply to *Dvu*Cas2, insofar as the equivalent Asp14 side chains are separated by 15.4 Å (Fig. 3). It also strikes us as implausible that other homodimeric Cas2 homologs could form the proposed composite metal-binding site with contributions from both protomers because the equivalent aspartates are separated by 12.8 Å in *Tth*1823 and by 10.8 Å in *Pfu*1117. In order for these aspartates to bind a bridging metal, the Cas2 proteins would need to undergo a major reorientation of their homodimer interfaces. For *Dvu*Cas2, at least, this would entail the disruption and remodeling of a large number of cross-protomer contacts. Beloglazova *et al.* (2008) also suggested that the α2–β4 loop of *Sso*1404 might be responsible for RNA substrate recognition by the Cas2 endonuclease. The equivalent segment is missing from *Dvu*Cas2.

It is worth considering that endoribonuclease activity might not be shared by all members of the Cas2 family and that at least some of the residues found to be essential for RNase activity in *Sso*1404 might have a structural role. This scenario would be plausible in *Dvu*Cas2, where we see that Tyr13 (which is conserved in all Cas2 homologs) is buried in the protein core, where it donates a hydrogen bond to

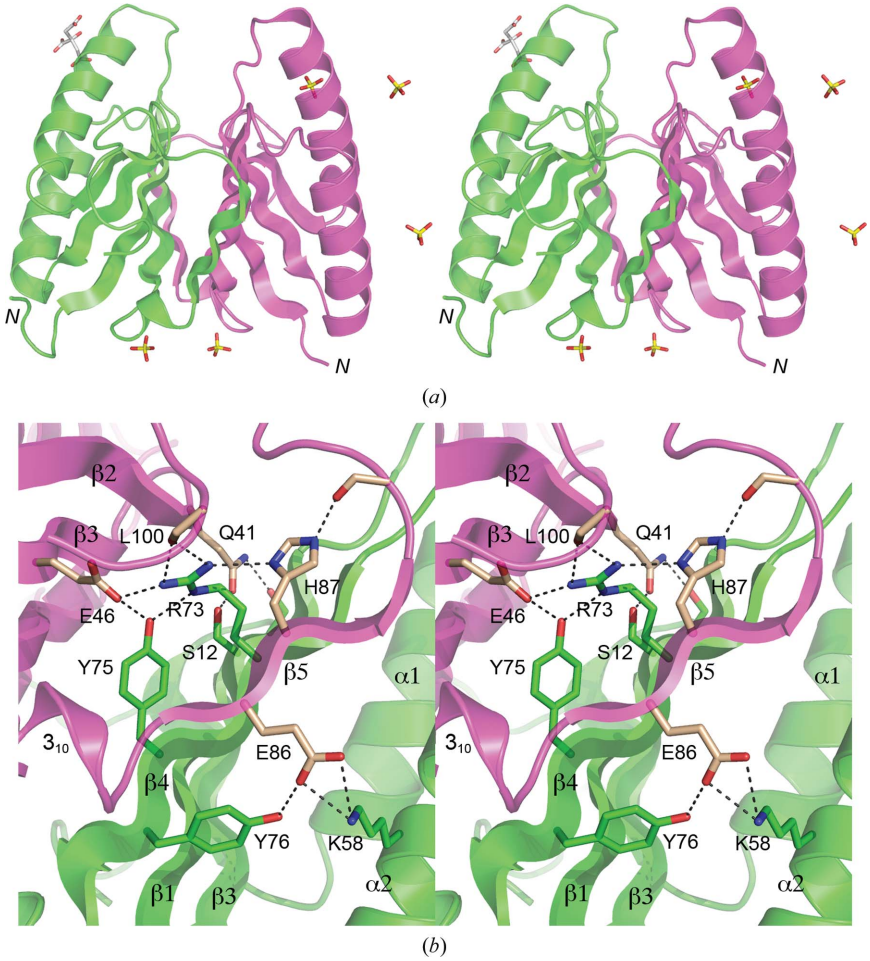

Figure 2
Stereoviews of the *Dvu*Cas2 dimer interface. (*a*) The folds of the *A* and *B* protomers are rendered in magenta and green, respectively. The N-termini are indicated. Five sulfates and a citrate located at various sites on the protein surface are shown as stick models. The two sulfate sites at the bottom of the image were refined as partially occupied by sulfate and partially by citrate; only the sulfates are shown for the sake of clarity. (*b*) This view highlights the hydrophilic cross-protomer side-chain interactions. The secondary-structure elements are labeled as in Fig. 1(*f*). Side chains of the *A* and *B* protomers that comprise the dimer interface are shown as stick models with beige and green C atoms, respectively. Ionic and hydrogen-bonding contacts of side-chain atoms at the dimer interface are indicated by dashed lines.

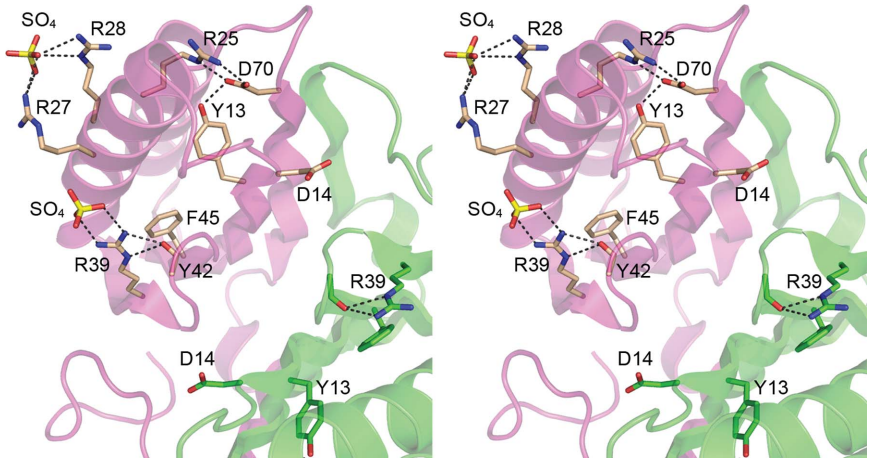

Figure 3
Disposition of *Dvu*Cas2 residues corresponding to those implicated in the endoribonuclease activity of Cas2 homologs. The folds of the *A* and *B* protomers are rendered in magenta and green, respectively. The side chains of the *A* and *B* protomers that correspond to the putative *Sso*1404 phosphodiesterase active-site residues (Fig. 1*f*) are shown as stick models with beige and green C atoms, respectively. Two sulfate anions docked on the surface of the *Dvu*Cas2 *A* protomer are also shown as stick models. Ionic and hydrogen-bonding interactions are indicated by dashed lines.

Asp70, which in turn makes a salt bridge to Arg25 (Fig. 3). Phe45, another invariant Cas2 residue, is buried in the hydrophobic core of the ferredoxin fold (Fig. 3). Neither Tyr13 nor Phe45 is disposed for a catalytic role. However, *Dvu*Cas2 Arg39 (equivalent to Arg31 in *Sso*1404) might be a candidate to interact with a nucleic acid because in one of the *Dvu*Cas2 protomers of the homodimer Arg39 coordinates a sulfate anion (a potential mimetic of a polynucleotide phosphate) *via* a bidentate salt bridge to the terminal guanidinium N atoms (Fig. 3). Note that Arg39 also contributes to the *Dvu*Cas2 fold in both protomers *via* a bifurcated hydrogen bond to the Tyr42 main-chain carbonyl (Fig. 3). Arg39 is conserved in *Tth*1823, *Sso*8090 and *Sso*1404, but is replaced by Trp in *Pfu*1117 (Fig. 1*f*). Another sulfate anion in the *Dvu*Cas2 structure is coordinated by Arg27 and Arg28 (Fig. 3). Arg28 (equivalent to Arg19 in *Sso*1404) is conserved as a basic residue in other Cas2 homologs, but Arg27 is not (Fig. 1*f*). We have been unable to convincingly demonstrate a metal-dependent endonuclease activity for purified *Dvu*Cas2 or to demonstrate its binding to ssRNA or ssDNA in a gel-shift assay format.

In summary, the 1.35 Å resolution crystal structure of *Dvu*Cas2 underscores a common fold for Cas2-family members, while revealing distinctive structural features of *Dvu*Cas2, especially at the homodimer interface. The *Dvu*Cas2 structure does not fit the current models of endonuclease catalysis proposed for *Sso*1404.

We thank Dr Yehuda Goldgury for assistance with data collection. This research was supported by NIH grant GM63611. SS is an American Cancer Society Research Professor.

References

Adams, P. D., Grosse-Kunstleve, R. W., Hung, L.-W., Ioerger, T. R., McCoy, A. J., Moriarty, N. W., Read, R. J., Sacchettini, J. C., Sauter, N. K. & Terwilliger, T. C. (2002). *Acta Cryst.* D**58**, 1948–1954.
Barrangou, R., Fremaux, C., Deveau, H., Richards, M., Boyaval, P., Moineau, S., Romero, D. A. & Horvath, P. (2007). *Science*, **315**, 1709–1712.
Beloglazova, N., Brown, G., Zimmerman, M. D., Proudfoot, M., Makarova, K. S., Kudritska, M., Kochinyan, S., Wang, S., Chruszcz, M., Minor, W., Koonin, E. V., Edwards, A. M., Savchenko, A. & Yakunin, A. F. (2008). *J. Biol. Chem.* **283**, 20361–20371.
Brouns, S. J., Jore, M. M., Lundgren, M., Westra, E. R., Slijkhuis, R. J., Snijders, A. P., Dickman, M. J., Makarova, K. S., Koonin, E. V. & van der Oost, J. (2008). *Science*, **321**, 960–964.
Emsley, P. & Cowtan, K. (2004). *Acta Cryst.* D**60**, 2126–2132.
Haft, D. H., Selengut, J., Mongodin, E. F. & Nelson, K. E. (2005). *PLoS Comput. Biol.* **1**, e60.
Hale, C. R., Zhao, P., Olson, S., Duff, M. O., Graveley, B. R., Wells, L., Terns, R. M. & Terns, M. P. (2009). *Cell*, **139**, 945–956.
Heidelberg, J. F. *et al.* (2004). *Nature Biotechnol.* **22**, 554–559.
Horvath, P. & Barrangou, R. (2010). *Science*, **327**, 167–170.
Karginov, F. V. & Hannon, G. J. (2010). *Mol. Cell*, **37**, 7–19.
Makarova, K. S., Grishin, N. V., Shabalina, S. A., Wolf, Y. I. & Koonin, E. V. (2006). *Biol. Direct*, **1**, 7.
Marraffini, L. A. & Sontheimer, E. J. (2008). *Science*, **322**, 1843–1845.
Marraffini, L. A. & Sontheimer, E. J. (2010). *Nature Rev. Genet.* **11**, 181–190.
Mojica, F. J., Diez-Villasenor, C., Garcia-Martinez, J. & Soria, E. (2005). *J. Mol. Evol.* **60**, 174–182.
Oost, J. van der, Jore, M. M., Westra, E. R., Lundgren, M. & Brouns, S. J. J. (2009). *Trends Biochem. Sci.* **34**, 401–407.
Otwinowski, Z. & Minor, W. (1997). *Methods Enzymol.* **276**, 307–326.
Pourcel, C., Salvignol, G. & Vergnaud, G. (2005). *Microbiology*, **151**, 653–663.
Sorek, R., Kunin, V. & Hugenholtz, P. (2008). *Nature Rev. Microbiol.* **6**, 181–186.
Terwilliger, T. C. (2000). *Acta Cryst.* D**56**, 965–972.
Terwilliger, T. C. (2003). *Acta Cryst.* D**59**, 38–44.